

# Initial conditions for disc galaxies

Paul J. McMillan<sup>1,2,3\*</sup> and Walter Dehnen<sup>1</sup>

<sup>1</sup>*Department of Physics & Astronomy, University of Leicester, Leicester, LE1 7RH, UK*

<sup>2</sup>*LAM, Observatoire Astronomique de Marseille Provence, 2 Place Le Verrier, F-13248 Marseille Cedex 4, France*

<sup>3</sup>*Rudolf Peierls Centre for Theoretical Physics, 1 Keble Road, Oxford, OX1 3NP, UK*

27 October 2018

## ABSTRACT

We present a general recipe for constructing  $N$ -body realizations of galaxies comprised of near-spherical and disc components. First, an exact spherical distribution function for the spheroids (halo & bulge) is determined, such that it is in equilibrium with the gravitational monopole of the disc components. Second, an  $N$ -body realisation of this model is adapted to the full disc potential by growing the latter adiabatically from its monopole. Finally, the disc is sampled with particles drawn from an appropriate distribution function, avoiding local-Maxwellian approximations. We performed test simulations and find that the halo and bulge radial density profile very closely match their target model, while they become slightly oblate due to the added disc gravity. Our findings suggest that vertical thickening of the initially thin disc is caused predominantly by spiral and bar instabilities, which also result in a radial re-distribution of matter, rather than scattering off interloping massive halo particles.

**Key words:** Methods:  $N$ -body simulations – Galaxies: kinematics and dynamics – Galaxies: haloes

## 1 INTRODUCTION

Generating an equilibrium  $N$ -body representation of a multi-component galaxy is of importance for a number of applications, for example the study of bars (e.g. Debattista & Sellwood 2000; Athanassoula 2002), warps (e.g. Ideta et al. 2000) and galaxy mergers, both minor (e.g. Mihos et al. 1995; Walker et al. 1996) and major (e.g. Heyl, Hernquist, & Spergel 1996; Naab, Burkert, & Hernquist 1999). Yet, constructing realistic equilibrium models is considerably difficult and in fact impossible rigorously, i.e. requires some sort of approximation.

Barnes (1988) introduced a “rather ad-hoc” method for constructing  $N$ -body models for a multi-component galaxy. He begins by constructing separate spherical equilibrium  $N$ -body King (1966) models for the halo and bulge, which are then superposed and allowed to relax into a new equilibrium over several dynamical times. Next, the gravitational potential of the disc is slowly imposed, causing both a flattening and a radial contraction of halo and bulge. Finally the disc component is populated with particles drawn from a Maxwellian distribution with the local mean and dispersion in agreement with the Jeans equations.

Hernquist (1993) introduced another method, which makes it possible to specify the density and velocity profiles of the various components in a straightforward way. In this method, the positions of all the particles in all components are determined first. This can be carried out easily since the desired density profiles are known. The Jeans equations are then used to find the velocity dispersions of

the various components, with those for the halo being found under the assumption that the potentials of disc and bulge can be approximated by their spherical average. Finally, individual velocities for all components are drawn from a locally Maxwellian distribution with the appropriate mean and dispersion velocities.

Boily, Kroupa, & Peñarrubia-Garrido (2001) extended this approach to include a non-spherical halo, but maintained the approximation to a Maxwellian distribution for the particle velocities. This method is not rigorous and Hernquist (1993) himself suggested that “In the future, it will likely be necessary to refine the basic approach as computer hardware and software permit simulations with particle numbers significantly in excess of those discussed here.” (he used  $N = 49\,152$  in his empirical tests).

Kazantzidis, Magorrian, & Moore (2004b) compared the properties of  $N$ -body haloes based on the Maxwellian approximation with those derived from an exact distribution function found through Eddington (1916) inversion. As their study clearly demonstrates, the Maxwellian approximation results in non-equilibrium effects and is inappropriate, for example, when modelling the tidal stripping of substructure in CDM haloes. Unfortunately, Eddington inversion only works for spherically symmetric equilibria and cannot be straightforwardly applied to the problem of finding the self-consistent distribution function of a multi-component system.

Therefore, Kuijken & Dubinski (1995) followed an alternative method, later expanded by Widrow & Dubinski (2005). They start from an analytical ansatz for the equilibrium distribution function of each component in isolation, written in terms of energy and angular momentum. In the case of the disc, the distribution function is also a function of the “vertical energy”  $E_z \equiv \frac{1}{2}v_z^2 + \Phi(R, z) - \Phi(R, 0)$ ,

\* E-mail: p.mcmillan1@physics.ox.ac.uk

which for orbits close to the disc plane is approximately conserved. These distribution functions are found for predetermined isolated density distributions. In the case of Kuijken & Dubinski (1995) these were a King (1966) model bulge, a lowered Evans model (Kuijken & Dubinski 1994) halo and an exponential disc. The combined model is then found by using these distribution functions in the combined gravitational potential of the entire model. The major problem with this approach is summed up by Widrow & Dubinski (2005) when they state that the combined model constructed in this way “may bare [*sic*] little resemblance to the corresponding isolated components, a situation which is cumbersome for model building”. This approach is also rather inflexible.

In this study, we therefore return to using Eddington inversion (in fact a generalisation thereof) for the near-spherical components but an analytic distribution function for the disc. Our method is detailed in Section 2, while Section 3 presents extended tests of the robustness and stability of the constructed  $N$ -body equilibria. Finally, Section 4 sums up and concludes.

## 2 THE NEW METHOD

Our method bears some relation to that of Barnes (1988), in that the non-spherically symmetric component (the disc), is grown adiabatically within the  $N$ -body halo. The bulge is assumed to be spherically symmetric, though it would be a relatively straightforward step to include a non-spherical bulge in a similar way to the disc. The process has three stages:

- (i) Creating an equilibrium initial  $N$ -body representation of the spherically symmetric components of the galaxy (halo and bulge) in the presence of an external potential field corresponding to the monopole (spherical average) of the desired disc potential.
- (ii) Evolving the  $N$ -body system by growing the non-monopole components of the disc potential adiabatically in a  $N$ -body simulation, in order to allow halo and bulge particles time to relax into the new potential.
- (iii) Replacing the external potential field representing the disc component with an  $N$ -body representation.

### 2.1 Creating the initial $N$ -body halo and bulge

We create an  $N$ -body realization of the spherically symmetric components of the system using Cuddeford’s (1991) method, an extension of the model by (Osipkov 1979) and (Merritt 1985), which in turn extended Eddington’s (1916) original inversion technique to obtain the distribution function for a spherical system with an isotropic velocity distribution.

Cuddeford considered distribution functions of the form

$$f(\mathcal{E}, L) = L^{2\alpha} f_0(Q). \quad (1)$$

Here,  $Q \equiv \mathcal{E} - L^2/2r_a^2$  as for Osipkov-Merritt models ( $\mathcal{E} \equiv \Psi - \frac{1}{2}v^2$ ,  $\Psi$  denoting the negative of the gravitational potential) with anisotropy radius  $r_a$ . The parameter  $\alpha$  is constrained to be greater than  $-1$ . As Cuddeford showed,  $f(Q)$  is related to the density by an Abel integral equation, which can (under the assumption that  $f(Q < 0) = 0$ ) be inverted to yield

$$f_0(Q) = \frac{\sin(n - \frac{1}{2} - \alpha)\pi}{\pi \lambda(\alpha) \eta(\alpha)} \frac{d}{dQ} \int_0^Q \frac{d^n \rho_{\text{red}}}{d\Psi^n} \frac{d\Psi}{(Q - \Psi)^{\alpha+3/2-n}}, \quad (2)$$

where  $n$  is defined as the largest integer equal to or less than  $\alpha + \frac{3}{2}$ , and where the “reduced density” is given as

$$\rho_{\text{red}} = \frac{(1 + r^2/r_a^2)^{\alpha+1}}{r^{2\alpha}} \rho, \quad (3)$$

while

$$\eta(\alpha) = \begin{cases} (\alpha + \frac{1}{2})(\alpha - \frac{1}{2}) \dots (\alpha + \frac{3}{2} - n), & \alpha > -\frac{1}{2} \\ 1 & -1 < \alpha \leq -\frac{1}{2}, \end{cases} \quad (4)$$

and

$$\lambda(\alpha) = 2^{\alpha+3/2} \pi^{3/2} \frac{\Gamma(\alpha+1)}{\Gamma(\alpha+3/2)}. \quad (5)$$

This distribution function produces a spherically symmetric system with a velocity distribution such that

$$\beta(r) \equiv 1 - \frac{\sigma_\theta^2}{\sigma_r^2} = \frac{r^2 - \alpha r_a^2}{r^2 + r_a^2}. \quad (6)$$

In the case where  $\alpha = 0$  this model reduces to an Osipkov-Merritt model. In the case where  $r_a \rightarrow \infty$ , the anisotropy of the halo is the same at all radii,  $\beta = -\alpha$ .

This approach has the advantage that the distribution function is exact for a spherically symmetric system, and thus remains in equilibrium, maintaining its original density profile. At no point is the assumption of a Maxwellian velocity distribution made. The only restrictions to this method are that  $\Psi = \Psi(r)$  is a monotonic function of radius (only); that  $\rho = \rho(r)$  and that the solution to equation (2) must be physical, i.e.  $f_0(Q) \geq 0$ . This allows us to use a wide range of different halo (or bulge) density profiles.

It is extremely useful that the derivation of equation (2) does not make the assumption that the potential of the system is that due to the density profile through the Poisson equation. This means that it is straightforward to generalise this approach to find the distribution function of a spherically symmetric component of a larger, spherically symmetric, system. The term  $\rho_{\text{red}}$  in equation (3) is replaced by the reduced density  $\rho_{\text{red},i}$  the reduced density of the component  $i$ ; the term  $\Psi$  in equation (3) always refers to the potential of the *entire* system.

In the model, the presence of the disc component is taken into account when calculating the distribution function of the halo and bulge. It is impossible to do this exactly using this method, as the disc is not spherically symmetric. The best approximation available in this case is to take the spherical average of the disc potential. Then the distribution functions of the bulge and halo are found in the total potential of the halo, bulge and fictitious spherically averaged disc. This prevents the radial contraction seen in the models constructed by Barnes (1988).

Finally, we shall briefly describe how we choose initial conditions from a model with distribution function of the form (1). First, we draw an initial position from the density in the usual way by inverting the cumulative mass profile for the radius. Secondly, we sample velocities by introducing pseudo-elliptical coordinates  $(u, \eta)$  in velocity space such that  $v_r = u \cos \eta$  and  $v_t = u(1 + r^2/r_a^2)^{-1/2} \sin \eta$ . Then we pick values for  $\eta$  and  $u$  at random from the distributions  $p(\eta) = \sin^{1+2\alpha} \eta$  and  $p(u) = u^{2+2\alpha} f_0(\Psi - \frac{1}{2}u^2)$ , using the rejection method for the latter.

### 2.2 Evolving the halo and bulge to adapt to the disc

The second stage of creating the model is to evolve  $N$ -body model of halo and bulge so that it is in equilibrium with the full disc potential, rather than with its spherical average. To this end we use

the  $N$ -body code *gyrfalcon*, which is based on Dehnen's (2000; 2002) force solver *falcon*— though the axisymmetry of the system means that a code based upon an expansion in spherical harmonics about the origin (such as the so-called self-consistent field codes, e.g. Hernquist & Ostriker 1992) would be well suited to this purpose.

The full potential of the disc,  $\Phi_{\text{disc}}(\mathbf{x})$  is grown from its spherical average  $\Phi_{\text{disc},0}(r)$  according to the formula

$$\Phi(\mathbf{x}, t) = \Phi_{\text{disc},0}(r) + A(t) [\Phi_{\text{disc}}(\mathbf{x}) - \Phi_{\text{disc},0}(r)], \quad (7)$$

where  $A(t)$  is a growth factor that goes from 0 at  $t = 0$  to 1 smoothly in a time-scale,  $t_{\text{grow}}$ , far longer than the dynamical time in the region of the disc. The halo and bulge are then allowed further time to relax completely under the influence of the disc potential.

This process causes changes to the density distribution of the halo. The spherically averaged density distribution is largely unchanged, but the halo and bulge are somewhat flattened, and the iso-density contours of both the halo and bulge become oblate. The degree of flattening is dependent on the details of the various components, a typical example is given in Section 3.

This stage is by some distance the slowest in the creating of the initial conditions. However it is still takes a relatively small fraction of the total CPU time of almost any scientifically interesting simulation. It should also be noted that up until this point the velocity distribution of the disc has not been a factor in the calculations, so the halo and bulge created by this process can be re-used in simulations with identical disc density profiles, but different disc kinematics.

### 2.3 Populating the disc

We start from the assumption that the motion of disc particles decouples into its components in the plane of the disc, and perpendicular to it. That is, we assume that the planar and vertical components of the total energy,  $E_{\parallel} \equiv \frac{1}{2}(v_R^2 + v_\phi^2) + \Phi(R, 0)$  and  $E_{\perp} \equiv \frac{1}{2}v_z^2 + \Phi(R, z) - \Phi(R, 0)$ , are both separately conserved. This assumption is usually excellent for orbits near the disc, for which always  $|z| \ll R$ . The potential  $\Phi$  here is, of course, the total potential of the system, i.e. that of the disc model plus that of the evolved  $N$ -body system. The first is computed as in Dehnen & Binney (1998), while the latter is approximated using a potential expansion (so-called SCF) method whereby ensuring axial symmetry by taking only  $m = 0$  and even  $l$  terms.

We make an ansatz for the disc distribution function, following the approach of Dehnen (1999b). As in that study, we first consider the simplest distribution function, i.e. that of a dynamically completely cold disc, in which all particles are on circular orbits. For a disc with density  $\rho = \Sigma(R) \delta(z)$  ( $\Sigma$  being the surface density), this can be written as (e.g. Dehnen 1999b)

$$f_{\text{cold}}(E_{\parallel}, L_z, z, v_z) = \frac{\Omega(R_{L_z}) \Sigma(R_{L_z})}{\pi \kappa(R_{L_z})} \delta(E_{\parallel} - E_c(R_{L_z})) \delta(z) \delta(v_z), \quad (8)$$

where  $\Omega(R)$  and  $\kappa(R)$  denote the angular and epicycle frequency at radius  $R$  and  $E_c(R)$  the energy of the circular orbit through  $R$ , while  $R_{L_z}$  is the radius of the circular orbit with angular momentum  $L_z$ . In order to obtain a warm disc distribution function, one may replace the  $\delta$ -functions in (8) by exponentials, resulting in a locally Maxwellian velocity distribution (e.g. Shu 1969; Kuijken & Dubinski 1995).

However, as demonstrated by Dehnen (1999b), it is better to

use the following alternative form for the cold-disc model before “warming” it up.

$$f_{\text{cold}}(E_{\parallel}, L_z, z, v_z) = \frac{\Omega(R_{E_{\parallel}}) \Sigma(R_{E_{\parallel}})}{\pi \kappa(R_{E_{\parallel}})} \delta(\Omega(R_{E_{\parallel}})[L_z - L_c(R_{E_{\parallel}})]) \delta(z) \delta(v_z), \quad (9)$$

where  $L_c(R)$  is the angular momentum of the circular orbit with radius  $R$  and  $R_{E_{\parallel}}$  the radius of the circular orbit with energy  $E_{\parallel}$ . Again, the warm disc distribution function is obtained by replacing the  $\delta$ -functions with exponentials (noting that  $z = 0$ ,  $v_z = 0$  means that  $E_{\perp} = 0$ ), giving

$$f_{\text{disc}}(E_{\parallel}, E_{\perp}, L_z) = \frac{\Omega(R_{E_{\parallel}}) \tilde{\Sigma}(R_{E_{\parallel}})}{(2\pi)^{3/2} \kappa(R_{E_{\parallel}})} \frac{1}{z_d \sigma_z(R_{E_{\parallel}})} \exp\left(-\frac{E_{\perp}}{\sigma_z^2(R_{E_{\parallel}})}\right) \times \frac{1}{\tilde{\sigma}_R^2(R_{E_{\parallel}})} \exp\left(-\frac{\Omega(R_{E_{\parallel}})[L_z - L_c(R_{E_{\parallel}})]}{\tilde{\sigma}_R^2(R_{E_{\parallel}})}\right). \quad (10)$$

Here,  $\tilde{\Sigma}(R)$  and  $\tilde{\sigma}_R(R)$  are sought such that the true surface-density and radial velocity-dispersion profiles of the  $N$ -body representation are those desired, to within an appropriate degree of accuracy, while the velocity dispersion in the vertical direction  $\sigma_z^2(R) = \pi G z_d \Sigma(R)$  with disc scale height parameter  $z_d$ .

Dehnen (1999b) argued that equation (10) gives a more useful distribution function than that of Shu (1969); he pointed that the warming of a disc can be described as an exponential in the radial action  $J_R$ . The radial action is more closely approximated by  $\Omega(R_{E_{\parallel}})[L_c(R_{E_{\parallel}}) - L_z]/\kappa(R_{E_{\parallel}})$  than by  $[E_{\parallel} - E_c(R_{L_z})]/\kappa(R_{L_z})$  (Dehnen 1999a). More practically, this distribution function has the advantage that the value of  $R_{E_{\parallel}}$  is generally a far better approximation to the mean radius of an orbit than  $R_{L_z}$ , which ensures that  $\Sigma(R)$  and  $\sigma_R(R)$  closely resemble  $\tilde{\Sigma}(R)$  and  $\tilde{\sigma}_R(R)$ , respectively. This choice of distribution function also extends to negative  $L_z$ , unlike that of Shu, allowing for a tail of counter-rotating stars.

When sampling from this distribution function, we attempt to minimise noise in the particle distribution by sampling points more regularly than random in phase space. We accomplish this by sampling orbits from the density distribution  $\tilde{\Sigma}(R)$ , then placing  $1 \ll N_{\text{sam}} \ll N_{\text{disc}}$  particles at points on each orbit. Finally, we iteratively adapt  $\tilde{\Sigma}(R)$  and  $\tilde{\sigma}_R(R)$  so that the actual surface density and velocity dispersion profile match the target profiles as closely as possible. The procedure for sampling the planar part of the phase-space positions is very similar to that proposed in Dehnen (1999b) and its details are as follows.

(i) Draw a radius from a thin disc with surface density  $\tilde{\Sigma}(R)$  (initially  $\tilde{\Sigma} = \Sigma$ ) and set  $E_{\parallel}$  to the energy of the circular orbit at  $R$ .

(ii) Draw a number  $\xi \in (0, 1)$  and determine

$$L_z = L_c(R) + \ln \xi \tilde{\sigma}_R^2(R)/\Omega(R). \quad (11)$$

If  $L_z \notin [-L_c(R), L_c(R)]$  go back to step (i).

(iii) Integrate the orbit with these values of  $E_{\parallel}$  and  $L_z$  for one radial period  $T_R$ , find the radial frequency  $\omega_R$ , and tabulate  $R(t)$  and  $\dot{R}(t)$  for that orbit. Evaluate the correction factor  $g_{\text{corr}} \equiv \kappa(R)/\omega_R$  (see Dehnen 1999b).

(iv) Given  $N_{\text{orb}} \approx N_{\text{disc}}^{1/2}$ , choose  $N_{\text{sam}}$  to be either of the two integers next to  $g_{\text{corr}} N_{\text{orb}}$  drawn with probabilities such that the mean equals  $g_{\text{corr}} N_{\text{orb}}$ . Next sample  $N_{\text{sam}}$  orbital phases  $t_i \in (0, T_R)$  and azimuth angles  $\phi_i \in (0, 2\pi)$ , and determine the corresponding phase-space points  $\{R_i, \phi_i, \dot{R}_i, \dot{\phi}_i\}$  from the orbit.

(v) Repeat steps (i) to (iv) until a total of  $N_{\text{disc}}$  disc particles have been sampled.

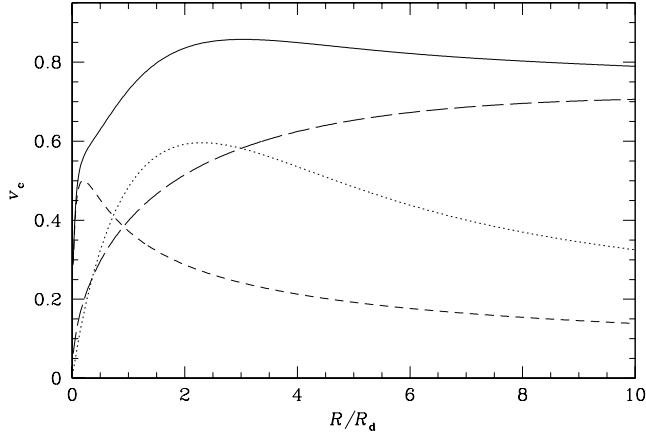


**Figure 1.** Rotation curve for the test galaxy model. The solid line is the net rotation curve, also shown are the contributions from the disc (*dotted*), bulge (*short-dashed*), and halo (*long-dashed*).

(vi) Finally, evaluate from the  $N_{\text{disc}}$  phase-space points the actual surface density and radial velocity dispersion,  $\Sigma_{\text{out}}$  and  $\sigma_{\text{out},R}$ , of the  $N$ -body model and adapt

$$\tilde{\Sigma}(R) \rightarrow \tilde{\Sigma}(R) \frac{\Sigma(R)}{\Sigma_{\text{out}}(R)}, \quad \tilde{\sigma}_R(R) \rightarrow \tilde{\sigma}_R(R) \frac{\sigma_R(R)}{\sigma_{\text{out},R}(R)}. \quad (12)$$

Then repeat the whole sampling procedure of steps (i) to (v) and iteratively adapt  $\tilde{\Sigma}(R)$  and  $\tilde{\sigma}_R(R)$  until no further improvement occurs.

If we use quasi-random, rather than pseudo-random, numbers in this procedure, it closely resembles the “quiet start” method (e.g. Sellwood 1987). Once this is done we determine the vertical component of each disc particle’s position and velocity. We assume that the local structure in the  $z$ -direction corresponds to that of an isothermal sheet with a constant vertical scale height,  $z_d$  (Spitzer 1942). This leads to a density throughout the disc  $\rho(R, z) \propto \text{sech}^2(z/z_d)$ .  $v_z$  is then drawn randomly from a normal distribution with  $\sigma_z^2 = \pi G \Sigma(R) z_d$ .

### 3 TESTING THE NEW METHOD

We test our approach using a model based loosely upon the Milky Way as modelled by Klypin, Zhao, & Somerville (2002). The disc is defined as having an exponential surface density profile with a vertical structure modelled by isothermal sheets, i.e.

$$\rho_d(R, z) = \frac{M_d}{4\pi R_d^2 z_d} \exp\left(-\frac{R}{R_d}\right) \text{sech}^2\left(\frac{z}{z_d}\right), \quad (13)$$

where  $M_d$  is the total disc mass,  $R_d$  is the disc scale radius, and  $z_d$  is a scale height (though it should be noted that this is not the e-folding height). The halo model is a truncated (Navarro et al. 1997, hereafter NFW) halo with initially spherical density distribution

$$\rho_h(r) = \rho_c \frac{\text{sech}(r/r_t)}{(r/r_h)(1 + r/r_h)^2}, \quad (14)$$

while the bulge is modelled with a Hernquist (1990) density profile

$$\rho_b(r) = \frac{M_b r_b}{2\pi r(r_b + r)^3}. \quad (15)$$

We choose units such that Newton’s constant of gravity  $G = 1$ ,  $R_d = 1$ , and  $M_d = 1$ . We take the disc scale height  $z_d = 0.1$ , the

bulge mass  $M_b = 0.2$  and scale length  $r_b = 0.2$ . Scaling these values to the Milky Way, taking  $R_d = 3.5$  kpc,  $M_d + M_b = 5 \times 10^{10} M_\odot$  (as in Klypin et al. 2002) gives a time unit  $\approx 14$  Myr, and thus a velocity unit of  $\sim 250 \text{ km s}^{-1}$ .

For the halo we take a scale radius  $r_h = 6$ , truncation radius  $r_t = 60$ , and mass  $M_h = 24$ , 79% of which is within the truncation radius. The rotation curve for this model (with velocities given in code units) is shown in Figure 1.

In all tests in which they were populated, the halo had 1 200 000 particles, the bulge 40 000 and the disc 200 000. This corresponds to each halo particle being 4 times more massive than a stellar particle. We use gravitational softening lengths of  $\epsilon = 0.02$  for disc and bulge particles, and 0.04 for halo particles. This choice ensures that the maximum force exerted by a single particle ( $\propto m_i/\epsilon_i^2$ ) is the same for all particles.

Simulations were performed with *gyrfalcON* with a minimum time-step of  $2^{-7}$ , and a block-step scheme with largest time step  $2^{-4}$ . Individual particle time-steps were adjusted such that on average the time-step

$$\tau_i = \min \left\{ \frac{0.01}{|\mathbf{a}_i|}, \frac{0.05}{|\Phi_i|} \right\}, \quad (16)$$

with  $\Phi_i$  and  $\mathbf{a}_i$  the gravitational potential and acceleration of the  $i$ th body in simulation units.

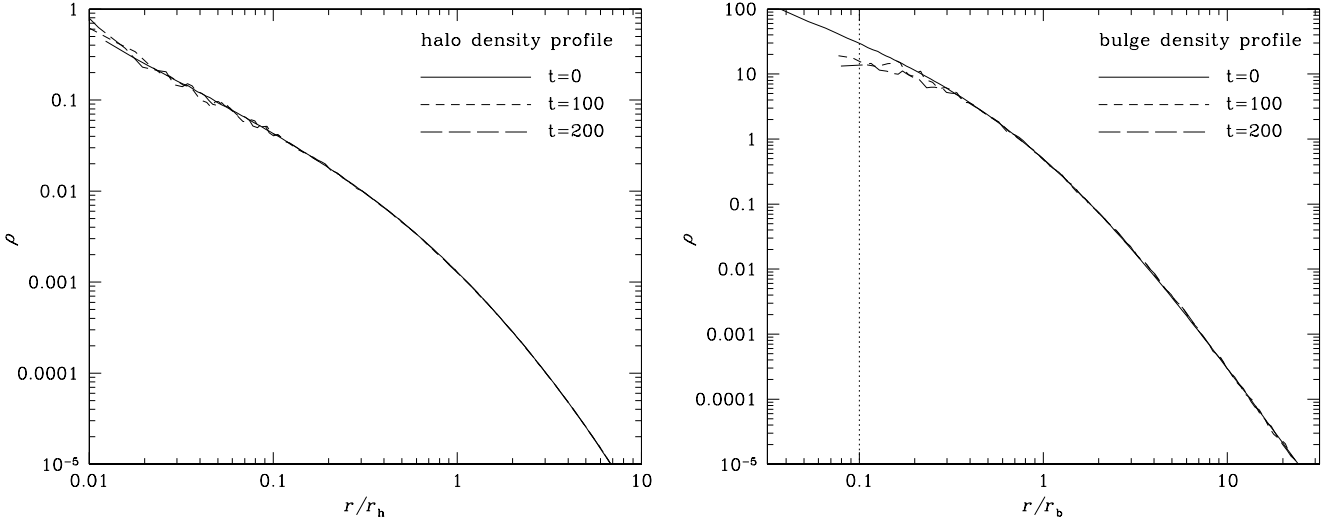
We first tested that the spherically symmetric components remain in equilibrium in the spherically-symmetrised potential. This was tested with various different choices for  $r_a$  and  $\alpha$  (equation (1)) in the halo, in order to ensure that Cuddeford inversion had been implemented correctly. The halo and bulge profiles remained consistent to within a few softening lengths of the centre, where softening and two-body relaxation have some small effect. This testing was also used to assess whether the time integration parameters were appropriate. Since energy was typically conserved to within 0.05% over 200 time units in these test simulations, we assume that the time integration is sufficiently accurate. For all further tests we only consider the isotropic case ( $\alpha = 0$ ,  $r_a \rightarrow \infty$ , so  $\beta = 0$  throughout the halo).

#### 3.1 Testing the disc growth

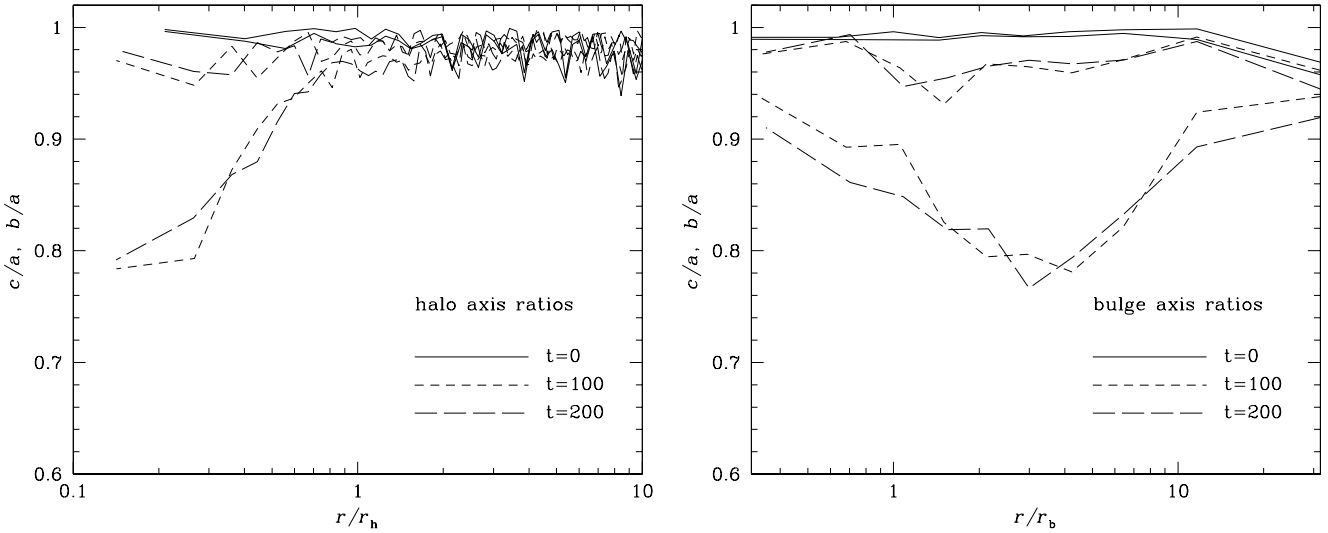
The next step was to ensure that the growth of the full disc potential from its monopole occurs without significant effect upon the radial density profile of the halo or bulge, or upon their kinematics, and to quantify the effect upon the shape of the resultant density distribution. The disc potential is grown as per equation (7), with a total growth time  $t_{\text{grow}} = 40$ . This is substantially longer than the dynamical time  $t_{\text{dyn}}$  in the vicinity of the disc (for instance at  $R = 3$ ,  $t_{\text{dyn}} \sim 6$ ).

Figure 2 shows the evolution of the density profiles of halo and bulge. Both are maintained to within a high degree of accuracy through the growth of the full potential, and then remain close to unchanged for a long period of time. The halo density is slightly raised in the inner  $\sim 0.02 r_h = 0.12$  and the bulge density is slightly lowered in the inner  $\sim 0.3 r_b = 0.06$ , in each case corresponding to only a few softening lengths. This is approximately the same as observed in simulations with no disc growth and is likely caused by mass segregation due to (artificial) two-body relaxation.

To quantify the flattening of halo and bulge due to the growth of the full disc potential, we determine the axis ratios of the halo and bulge as a function of radius. To this end, we first estimate the local density at each particle’s position by the nearest-neighbour



**Figure 2.** Spherically averaged density profile of the halo (*left*) and bulge (*right*), shown just before growth of the full disc potential ( $t = 0$ ), and at 100 and 200 time units. The disc component was not populated in this simulation. The density profiles remain more or less unchanged by the growth of the full potential, except at radii only slightly larger than the respective softening length ( $\epsilon_h = 0.0066r_h$  and  $\epsilon_b = 0.1r_b$ , indicated by the dotted vertical line).



**Figure 3.** Minor and intermediate axis ratios ( $c/a < b/a$  respectively), for both the halo (*left*) and bulge (*right*) in the same simulations as in Fig. 2. Particles are binned in density, and the values plotted here are the axis ratios of these bins against their median radius. Deviations from sphericity ( $c/a = b/a = 1$ ) at  $t = 0$  are entirely due to discreteness noise.

method of Casertano & Hut (1985), using the 15 nearest neighbours (of the same component). Next, we bin the particles in estimated density and evaluate the axis ratios in each bin as the square roots of the ratios of the eigenvalues of the moment-of-inertia tensor<sup>1</sup>. Figure 3 plots the axis ratios such obtained for halo and bulge versus the radius (the median radius of the corresponding density bin). Obviously, there is some small effect on the bulge and halo

shape from the growth of the disc. In both cases the shortest ( $c$ ) axis is very close to the  $z$ -axis as expected. The degree of flattening is relatively modest, with  $c/a \approx 0.8$  in the most flattened shells. In the case of the halo this is within the inner  $\sim 0.3r_h = 1.8R_d$ . In the case of the bulge the most flattened shells are at  $\sim 3r_b = 0.6R_d$ . The bulge is less flattened at smaller radii because the disc is of finite thickness (scale height  $z_d = 0.1R_d$ ), which means that the full potential is less flattened – when compared to the spherical average – in the inner parts of the bulge than in the outer. The same effect would be observable in the halo with sufficient resolution.

<sup>1</sup> In the literature one often finds axis ratios computed for bins in spherical radius (e.g. Kazantzidis et al. 2004a). This not only requires accurate knowledge of the centre position, but more importantly results in a substantial bias (because of the usage of spherical symmetry). For a triaxial body, for example, the axis ratios at small radii are drastically overestimated (Athanasoula 2007). Binning in potential energy gives somewhat better but still unsatisfactory results (since the gravitational potential is less flattened than the density).

For both halo and bulge Figure 4 shows the evolution of the radial profile of the velocity anisotropy parameter  $\beta$  as determined from spherical shells. Both components are initially isotropic and, to within numerical accuracy, remain so during and well after the growth of the full disc potential.

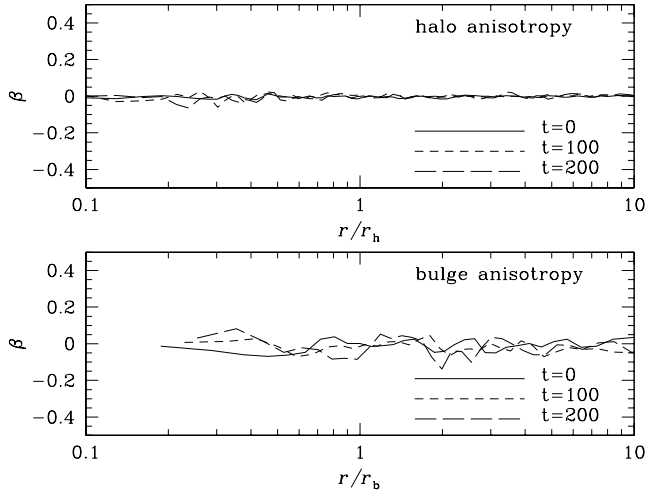


**Figure 4.** Anisotropy parameter  $\beta$ , determined from spherical shells, plotted against radius for the halo and bulge in the same simulations as in Fig. 2. Initial conditions were defined as having  $\beta = 0$  and variation from that at  $t = 0$  is due to discreteness noise.

### 3.2 Testing the disc model

Before testing the full compound galaxy, we test the disc model in isolation, i.e. we follow the evolution of the populated disc component in the static external potential  $\Phi(R, z)$ , the cylindrically-symmetrised potential in which the distribution function of the disc was constructed. The purpose of this test is to ensure that the approximate nature of our disc distribution function (the assumption that the planar and vertical energies are separately conserved) does not compromise our approach, i.e. that the disc  $N$ -body model is close to equilibrium.

The main difficulty here is that we want the disc model to be stable to axisymmetric perturbations, but not to non-axisymmetric instabilities, such as spiral waves and bar modes, both of which one would expect to see. These instabilities cause redistribution of the mass of the disc in both the  $R$  and  $z$  directions (e.g. Hohl 1971; Athanassoula & Misiriotis 2002). In the tests presented here, we prevent non-axisymmetric modes from growing by a technique pioneered by Athanassoula (private communication): the azimuth of every disc particle is randomised after every block-step, thus destroying any coherent non-axisymmetric perturbation.

The distribution function defined by equation (10) allows for many possible  $\sigma_R(R)$ . In practise our current implementation restricts the possibilities to either  $\sigma_R \propto \exp(-R/R_\sigma)$ , or  $\sigma_R$  is such that the Toomre (1964) stability parameter

$$Q \equiv \frac{\sigma_R \kappa}{3.36 G \Sigma} \quad (17)$$

is constant throughout the disc (this should not be confused with the Osipkov-Merritt  $Q$  in equation (1)). A stellar disc is known to be unstable to axisymmetric waves if Toomre's  $Q < 1$ .

We test two models, one with constant  $Q = 1.2$ , and one with  $\sigma_R \propto \exp(-R/2R_d)$  (i.e.  $R_\sigma = R_d/2$  so that  $\sigma_R^2 \propto \Sigma$ ), with the constant of proportionality defined such that  $Q(R = R_\sigma) = 1.2$ . The two give qualitatively similar results, so only the results from the latter distribution function are shown in Fig. 5 for simplicity. The surface density of the disc model is preserved to within the inner  $\sim 0.1 - 0.2R_d$ , and out to beyond  $6R_d$ . The radial velocity dispersion  $\sigma_R$  is preserved over a similar range.

In the middle panel of Fig. 5, we plot the r.m.s. value of  $z$  as

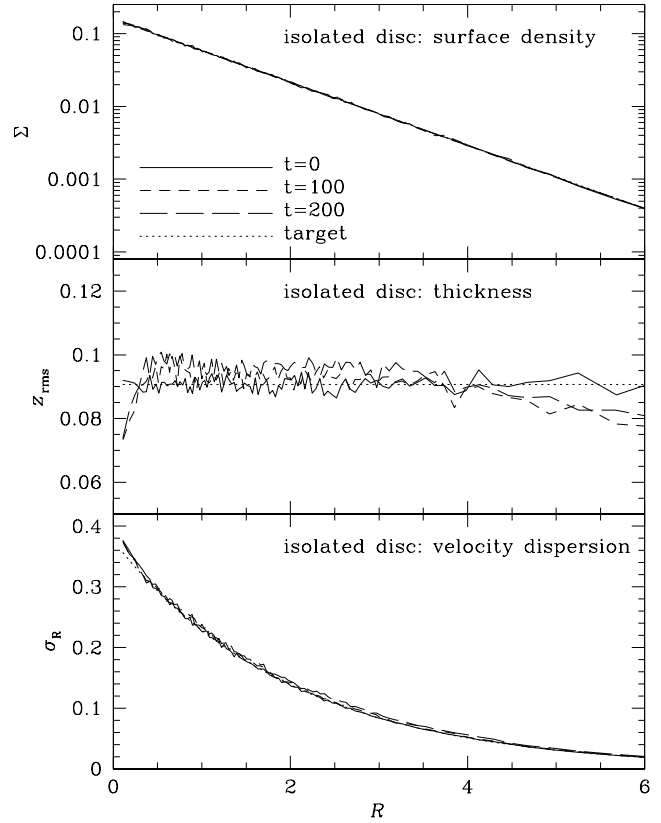


**Figure 5.** Radial profiles of surface density (top), thickness (middle), and radial velocity dispersion (bottom) for an isolated disc model. The randomising-azimuth method has been used to prevent the growth of bar or spiral modes.

a measure of the disc thickness. For a disc with  $\rho \propto \text{sech}^2(z/z_d)$  one expects  $z_{\text{rms}} = \pi z_d / \sqrt{12} \approx 0.907 z_d$ , indicated by a dotted line. The disc thickness remains near constant in the range  $0.3 \lesssim R \lesssim 4$ , with a slight warming which can reasonably be attributed to particle softening. The disc becomes somewhat flattened in its very inner ( $\sim 0.3R_d$ ) and outer ( $R > 4R_d$ ) parts. This is presumably caused by too low initial  $z$ -velocities, which were assigned assuming that the vertical force is dominated by the local disc. In the inner parts of the disc, the bulge has a non-negligible contribution to the vertical force field, and in the outer parts the local disc is very tenuous, so the contribution of the halo (and the monopole of the disc) to the vertical force field is significant. It should also be noted that the approximation that the planar and vertical motion decouple is worst in the inner parts of the disk, which may well contribute to the flattening there.

### 3.3 Testing the full model

#### 3.3.1 A constrained model

Finally we test the complete compound model. First we wish to examine the behaviour of the system in the absence of bar or spiral instabilities. In order to do so, we utilise the same method of randomising the azimuth (of disc particles only) as in Section 3.2.

However, using this method with a live halo and bulge is not straightforward, since a live  $N$ -body simulation will often drift slightly from its original centre. When this happens the disc will be pulled in same the direction as the inner halo, so that randomis-

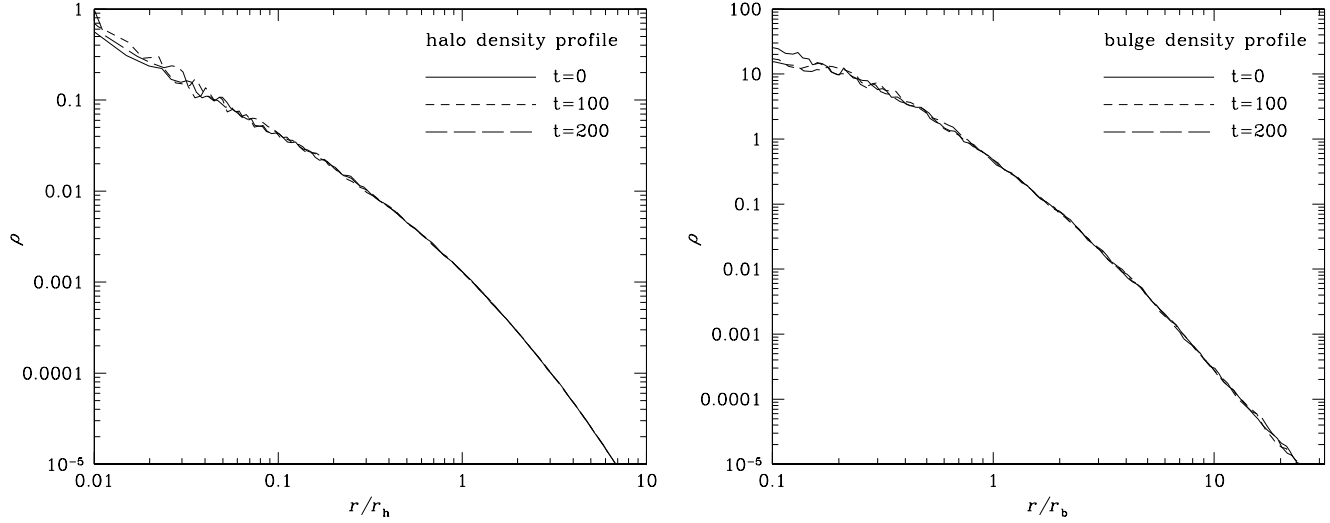


**Figure 6.** Spherically averaged density profile of the halo (*left*) and bulge (*right*) in a fully populated simulation with non-axisymmetric perturbations suppressed (see text). The profiles are shown at  $t = 0$ , when the full  $N$ -body model was populated but before it has evolved; and at two times during the full  $N$ -body simulation. Symmetry about the origin was enforced, to avoid numerical difficulties relating to off-centring.

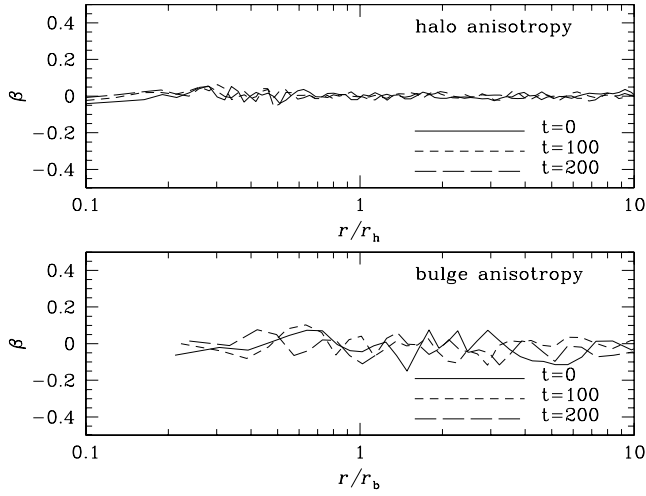


**Figure 8.** Anisotropy parameter  $\beta$ , as determined from spherical shells, vs. radius for the halo and bulge in the same simulations as Figs. 6 & 7.

ing azimuths around the origin would alter the model structure. In order to prevent such a drift, we employed another symmetrisation method: the distribution of particles in halo and bulge was kept reflection symmetric about the origin at all times. To this end, we treated particles in bulge and halo as pairs and enforced, initially and after each time step (during both the disc growth and the fully populated simulation), that for each pair positions and velocities both add up to zero.

In this test we set the velocity dispersion  $\sigma_R$  of the disc such that Toomre's  $Q = 1.2$  at all radii. The full disc potential was grown over a period  $t_{\text{grow}} = 40$ , as in Section 3.1, and then kept in place for a time  $t_{\text{hold}} = 20$  to ensure that the halo and bulge had fully relaxed in its presence. Only then was the disc populated with particles. Simulations were then run to observe the evolution over another 200 time-units. Times quoted in Figs. 6-9 take  $t = 0$  to be the time when the fully populated simulation begins (*not* the start of the growth of the full disc potential, as in Section 3.1).

Figures 6 and 7 show that the properties of the halo and

bulge are maintained to within a high degree of accuracy throughout the simulation. The halo density is slightly raised in the inner  $\sim 0.02r_h = 0.12$  and the bulge density is slightly lowered in the inner  $\sim 0.3r_b = 0.06$ , much as they were in simulations with an unpopulated disc (Fig. 2). Both components remain isotropic (with some noise, Fig. 8), and while they are non-spherical, they do not become significantly more or less aspherical over the course of the simulation (Fig. 7).

Figure 9 (top panel) shows that the surface density of the disc is nearly unchanged at all radii throughout the entire simulation. Also the disc thickness remains near constant over the full radial range. The small deviations are similar to those observed for the disc in isolation (Fig. 5). In particular, the disc does not thicken up as one might expect from heating due to collisions with (more massive) interloping halo particles. This is probably a side effect of the randomisation of the azimuthal angle of the disc particles. This randomisation has the effect that disc particles are rarely close to any halo particle crossing the disc for more than one time step.

The radial velocity dispersion  $\sigma_R$  in the disc (Fig. 9, bottom panel) is nearly unchanged in the range  $0.5 < R < 3$ . In the outer parts of the disc there is some variation, but no consistent warming or cooling. In the inner parts of the disc there is a clear increase in  $\sigma_R$ . This warming clearly does not affect the density distribution. It can reasonably be attributed to the facts that the decoupling of the vertical and planar motion is a poor approximation in the inner disc, and that, while the choice of a distribution function with constant  $Q$  can be useful in that it avoids the inner parts of the disc being very hot, it does lead to the velocity dispersion being unrealistically low at the very inner radii.

### 3.3.2 Unconstrained tests

Finally we run simulations in which the galaxy model is unconstrained from the moment the disc component is populated. This means that the disc component is free to develop bar modes and other instabilities.

In Fig. 10 we plot the surface density profiles of discs with various initial  $\sigma_R$  profiles. In each case  $\sigma_R$  was defined such that  $Q$  was constant across the disc. Simulations are shown with  $Q = 1.2, 2, 3$ ,

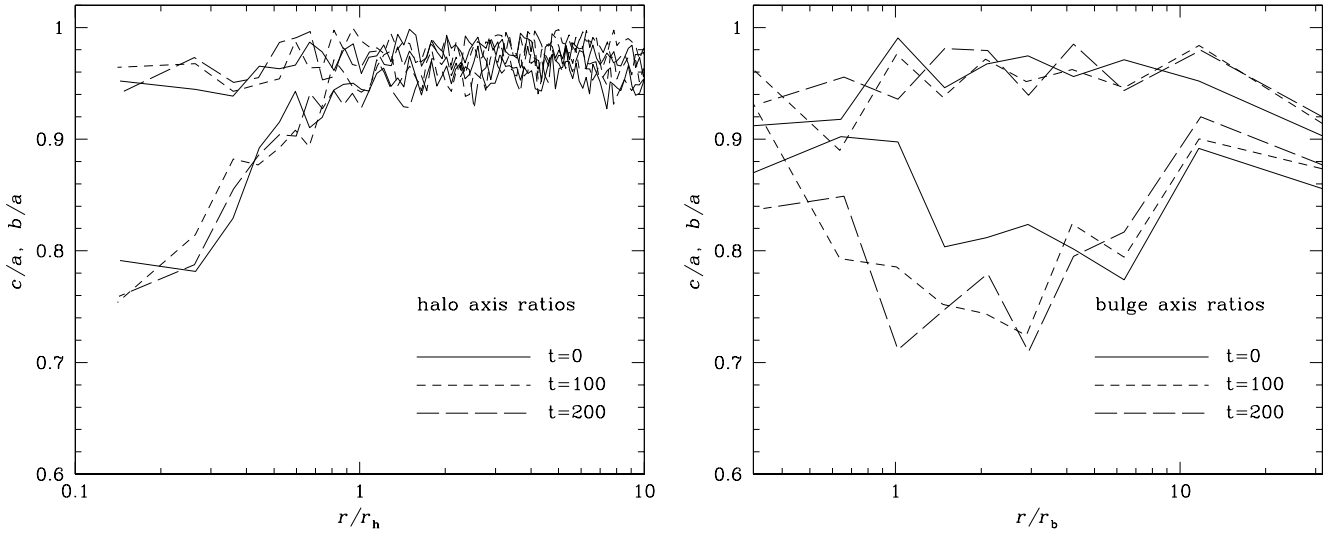


**Figure 7.** Minor and intermediate axis ratios ( $c/a < b/a$  respectively), for both the halo (left) and bulge (right) in the same simulations as in Fig. 6. Particles are binned in density, and the values plotted here are the axis ratios of these bins against their median radius.

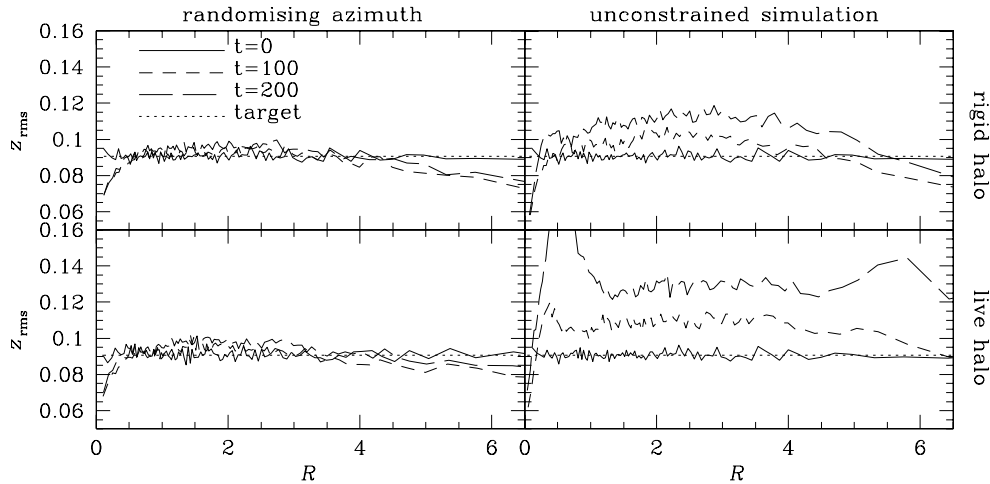


**Figure 13.** Evolution of the disk thickness in four different simulations: constrained (by randomising the azimuth) and unconstrained, with rigid or live halo. In all cases, the initial velocity dispersion of the disc was set such that  $Q = 1.2$  everywhere. The lower-left panel corresponds to the middle panel of Fig. 9 (but note the different scales).

and 4. For hotter discs (larger  $Q$ ), it becomes increasingly difficult to iterate the particle positions such that the surface density is close to that desired, using the method described in Section 2.3. This is why the initial surface density of the  $Q = 4$  disc (and to a lesser extent the  $Q = 3$  disc) is not an exponential in radius. It should also be noted that the motivation of warming an initially cold distribution function is increasingly invalid as the disc becomes hotter. Moreover, such hot axisymmetric discs are less realistic, given the observed fraction of barred galaxies (which cannot form from such hot discs).

It has long been recognised that numerical simulations of cool discs are much more susceptible to bar formation than those of warm discs (e.g. Hohl 1971). This is what we observe in our models. The scatter plot of particle positions for the  $Q = 1.2$  case, Figure 11, shows spiral structure forming within 50 time units, and the formation of a strong bar within 100. This has the effect of substantially altering the surface density profile, dramatically increasing the disc's surface density in the inner  $\sim 0.3$  scale lengths (as seen

in Fig. 10). The  $Q = 3$  disc shows no signs of developing spiral structure within 200 time units (Fig. 12), and the density profile remains nearly unchanged throughout the simulation.

### 3.3.3 On the origin of disc thickening

It is instructive to compare the disc thickening in the four different cases we have looked at in this study (populated/rigid halo; randomised azimuth/unconstrained model), see Figure 13. Simulations which are constrained so that non-axisymmetric modes are suppressed show hardly any disc thickening, strongly suggesting that the dominant cause of disc thickening in our models is the action of non-axisymmetric modes within the disc, rather than the impact of halo particles crossing the disc. Athanassoula (2002) showed that a populated halo can stimulate bar growth by absorbing angular momentum (which a rigid halo cannot). This is a likely explanation for the greater increase in disc thickness seen in the unconstrained



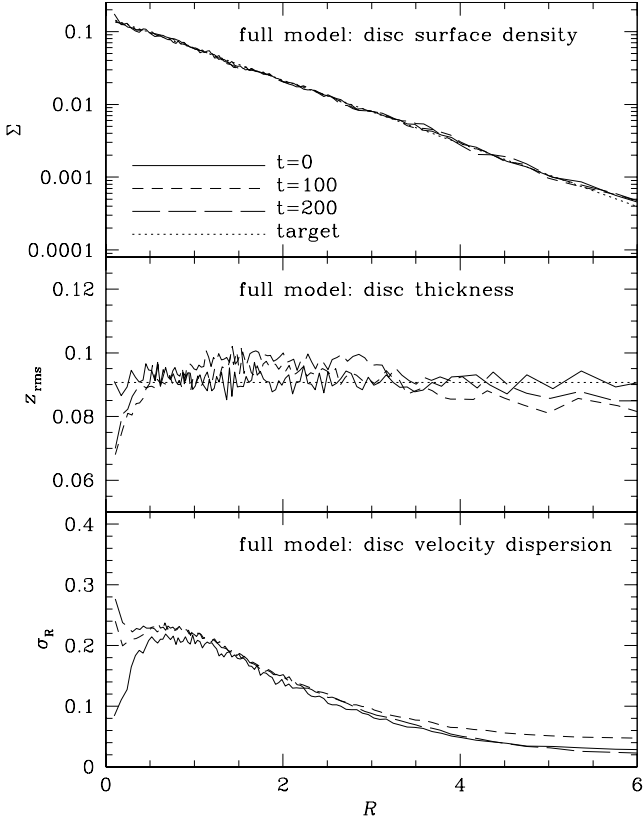


**Figure 9.** Radial profiles of surface density (*top*), thickness (*middle*), and radial velocity dispersion (*bottom*) of the disc component in a full  $N$ -body model, whose halo and bulge properties are shown in Figs. 6 to 8. The randomising-azimuth method has been used to prevent the growth of bar or spiral modes (see text).

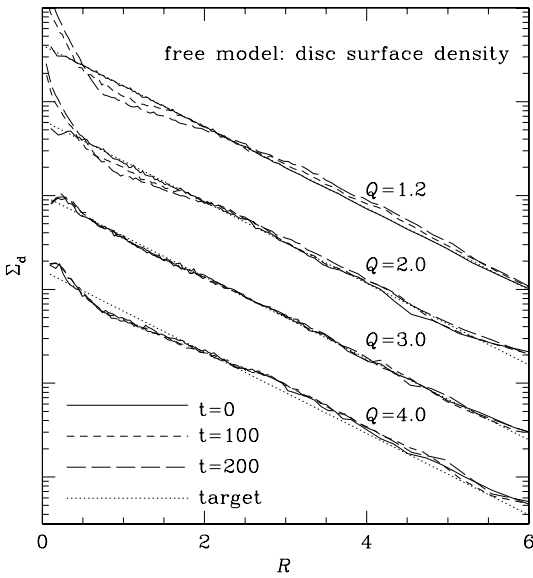


**Figure 10.** Surface density profiles for the discs in unconstrained simulations with four different values of Toomre's  $Q$  initially. Results for the different simulations are offset by a constant.

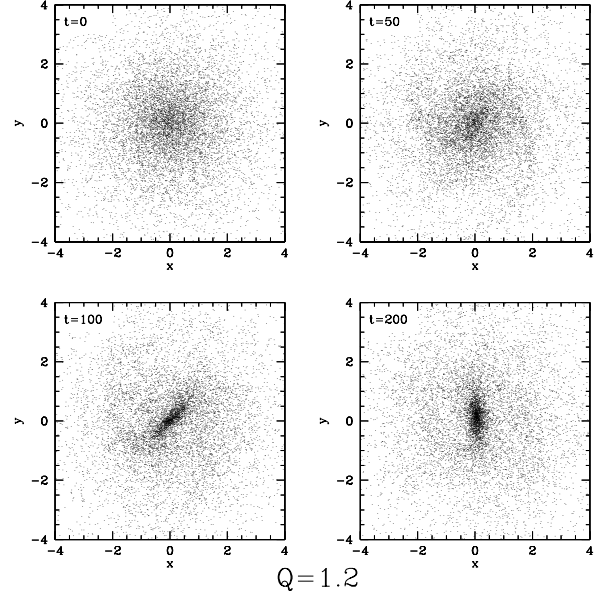


**Figure 11.** Scatter plot of disc particle positions in the  $x$ - $y$  plane at various times in an unconstrained simulation with initial  $Q = 1.2$ . Only 1 in every 20 particles is plotted, in the interests of clarity.

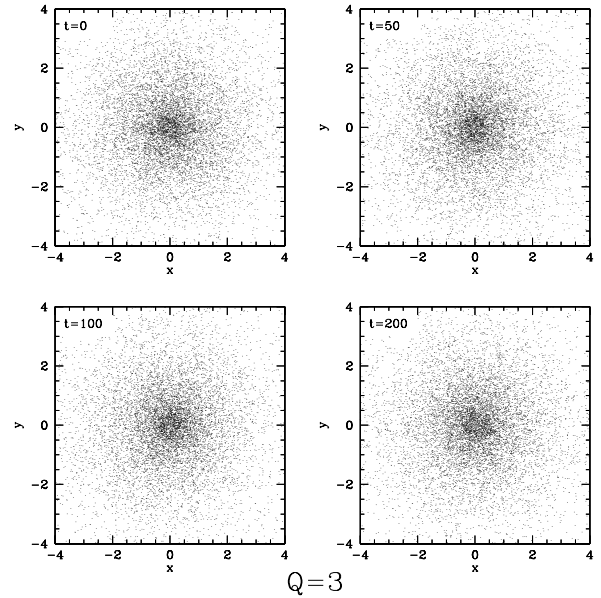


**Figure 12.** Scatter plot of disc particle positions in the  $x$ - $y$  plane at various times in an unconstrained simulation with initial  $Q = 3$ . As in figure 11, only 1 in every 20 particles is plotted.

simulation with live halo compared to that with a rigid halo (right panels in Fig. 13).

Possibly the randomisation of the disk particles' azimuths is also a direct cause of a reduction in disc thickening, because of the rapid jumps it causes in the disk particles' positions (rather than just an indirect cause, through preventing non-axisymmetric instabilities). Why this would be the case, however, is unclear.

#### 4 CONCLUSIONS

We have described and tested a new method for constructing an equilibrium  $N$ -body representation of a galaxy with halo, disc and bulge components.

We have used a distribution function for the halo and bulge based upon Cuddeford (1991) inversion, while the distribution function of the disc is based on the work of Dehnen (1999b). One advantage over previous methods is that our method avoids the use of a Maxwellian approximation, and produces models which tend to stay very close to their original states, though non-axisymmetric instabilities develop in the disc if it is unconstrained and reasonably dynamically cold.

Another advantage of our method is that the density distributions of the various components are straightforward to prescribe. That is, the way the models are constructed guarantees that the equilibrium  $N$ -body model has bulge, halo, and disc components the density profiles (as well as the velocity-anisotropy profiles) of which follow the target models very closely. Having said that, we have little control with our method over the degree of non-sphericity of halo and bulge, introduced by the disc's gravitational potential. We find that typically bulge and halo are mildly oblate (axis ratio  $\sim 0.8$ ) in the region dominated by the disc.

The choice of disc distribution function, while physically motivated, and clearly in equilibrium (though potentially unstable to non-axisymmetric modes), causes problems when creating a warm disc (Toomre's  $Q \gtrsim 4$ ) since it becomes increasingly difficult to tailor the distribution function to the desired density and velocity dispersion profiles. However, we are not aware of any other method to create such warm  $N$ -body disc with a truly exponential surface density profile.

We performed several tests to validate that the  $N$ -body model created by our method meets our expectations. These tests suggest that the growth of the disk thickness is predominantly driven by non-axisymmetric modes in the disc itself rather than direct interactions with halo particles.

The computer programs generated in the course of this project will be publicly available under the NEMO computer package ([www.astro.umd.edu/nemo](http://www.astro.umd.edu/nemo)).

#### ACKNOWLEDGEMENT

We are grateful for many useful discussions with Lia Athanassoula. PJM acknowledges support by the UK Particle Physics and Astronomy Research Council (PPARC) through a Research Student Fellowship and by an EU Marie Curie Fellowship. Astrophysics research at the University of Leicester is also supported through a PPARC rolling grant.

#### REFERENCES

- Athanassoula E., 2002, *ApJL*, 569, L83  
 Athanassoula E., 2007, *MNRAS* accepted, [astro-ph/0703184](http://arxiv.org/abs/astro-ph/0703184)  
 Athanassoula E., Misiriotis A., 2002, *MNRAS*, 330, 35  
 Barnes J. E., 1988, *ApJ*, 331, 699  
 Boily C. M., Kroupa P., Peñarrubia-Garrido J., 2001, *NewA*, 6, 27  
 Casertano S., Hut P., 1985, *ApJ*, 298, 80  
 Cuddeford P., 1991, *MNRAS*, 253, 414  
 Debattista V. P., Sellwood J. A., 2000, *ApJ*, 543, 704  
 Dehnen W., 1999a, *AJ*, 118, 1190  
 Dehnen W., 1999b, *AJ*, 118, 1201  
 Dehnen W., 2000, *ApJL*, 536, L39  
 Dehnen W., 2002, *Journal of Computational Physics*, 179, 27  
 Dehnen W., Binney J. J., 1998, *MNRAS*, 294, 429  
 Eddington A. S., 1916, *MNRAS*, 76, 572  
 Hernquist L., 1990, *ApJ*, 356, 359  
 Hernquist L., 1993, *ApJS*, 86, 389  
 Hernquist L., Ostriker J. P., 1992, *ApJ*, 386, 375  
 Heyl J. S., Hernquist L., Spergel D. N., 1996, *ApJ*, 463, 69  
 Hohl F., 1971, *ApJ*, 168, 343  
 Ideta M., Hozumi S., Tsuchiya T., Takizawa M., 2000, *MNRAS*, 311, 733  
 Kazantzidis S., Kravtsov A. V., Zentner A. R., Allgood B., Nagai D., Moore B., 2004a, *ApJL*, 611, L73  
 Kazantzidis S., Magorrian J., Moore B., 2004b, *ApJ*, 601, 37  
 King I. R., 1966, *AJ*, 71, 64  
 Klypin A., Zhao H., Somerville R. S., 2002, *ApJ*, 573, 597  
 Kuijken K., Dubinski J., 1994, *MNRAS*, 269, 13  
 Kuijken K., Dubinski J., 1995, *MNRAS*, 277, 1341  
 Merritt D., 1985, *MNRAS*, 214, 25P  
 Mihos J. C., Walker I. R., Hernquist L., Mendes de Oliveira C., Bolte M., 1995, *ApJL*, 447, L87  
 Naab T., Burkert A., Hernquist L., 1999, *ApJL*, 523, L133  
 Navarro J. F., Frenk C. S., White S. D. M., 1997, *ApJ*, 490, 493  
 Osipkov L. P., 1979, *Pisma Astronomicheskii Zhurnal*, 5, 77  
 Sellwood J. A., 1987, *ARAA*, 25, 151  
 Shu F. H., 1969, *ApJ*, 158, 505  
 Spitzer L. J., 1942, *ApJ*, 95, 329  
 Toomre A., 1964, *ApJ*, 139, 1217  
 Walker I. R., Mihos J. C., Hernquist L., 1996, *ApJ*, 460, 121  
 Widrow L. M., Dubinski J., 2005, *ApJ*, 631, 838